Non-Euclidean geometry model for chemo-mechanical coupling in self-assembled polymers towards dynamic elasticity

Ziyu Xing[a], Haibao Lu[a,*], Dong-Wei Shu[b] and Yong-Qing Fu[c,*]

[a]National Key Laboratory of Science and Technology on Advanced Composites in Special Environments, Harbin Institute of Technology, Harbin 150080, China

[b]School of Mechanical and Aerospace Engineering, Nanyang Technological University, 50 Nanyang Avenue, 639798, Singapore

[c]Faculty of Engineering and Environment, University of Northumbria, Newcastle upon Tyne, NE1 8ST, UK

[*]Corresponding author, E-mail: luhb@hit.edu.cn and richard.fu@northumbria.ac.uk

Abstract: Self-assembly plays a fundamental role to determine thermodynamic properties of polymer systems, e.g., resulting in the formation of dynamically cross-linked networks with varied elasticity. However, the working principle of chemo-mechanical coupling between the self-assembly and elasticity of polymers is complex and has not been well understood. In this study, a non-Euclidean geometry model incorporating thermodynamics of microphase separation is proposed to understand the chemo-mechanical coupling in self-assembled triblock polymers. The thermodynamic separation of microphases, which is resulted from the self-assembly of polymeric molecules, is formulated using a non-Euclidean geometry equation, of which the geometrical parameters are applied to characterize the topologies of self-assembled and cross-linked networks. The non-Euclidean geometry model is further employed to describe chemo-mechanical coupling between the self-assembled

network and dynamic elasticity of the triblock polymers, based on the rubber elasticity theory. Effectiveness of the proposed model is verified using both finite-element analysis and experimental results reported in literature. This study provides a new geometrical approach to understand the mechanochemistry and thermodynamics of self-assembled block polymers.

Keywords: hydrogel; self-assembled; Non-Euclidean geometry

1. Introduction

The unique performance of many biological matters in nature comes from their self-assembly properties [1-3]. Inspired from self-assembly, many artificial polymers have been developed with superior structure-property performance, achieving good mechanical, optical and thermodynamic properties [4-9]. Self-assembled polymers have been widely used in stretchable sensors [10], chemical fuels [11], living cells [12], nanoarchitectonics and biometallohydrogels [13,14], mainly attributed to their high designabilities and compatibilities. Many of these polymers have excellent mechanical properties of both high stretchability and strength [15-19]. However, their working principles and constitutive relationships between chemical self-assembly and mechanical elasticity have not been well understood owing to the complexly chemo-mechanical coupling effects.

Polymers can be easily tailored to achieve desirable physical properties by grafting various types of molecules onto their main/side chains or functional groups [20-25]. However, self-assembly of molecules often results in microphase separation [15-19,26,27], which is determined by the self-assembled network. Meanwhile,

thermodynamics of microphase separation plays an essential role to influence the mechanical performance of self-assembled polymers [4,28,29], and there is a complex thermo-mechano-chemical coupling among their microphase separation, mechanical behavior and self-assembly. It is critical to explore the working principle and constitutive relationship between self-assembly and microphase separation in order to fully understand the thermo-mechano-chemical coupling effect of the self-assembled polymers [29-31].

Self-assembled polymers are composed of different molecular segments [32-35], which enable them with unique thermodynamics of microphase separations for application in self-assembly [27,36]. Small angle neutron scattering experiments have revealed that there are many micelles in these block polymers undergoing microphase separations due to the hydrophilic properties of the molecular segments [37-39]. Take an example of PNIPAm-PDMA (PNIPAm: poly(N-isopropylacrylamide); PDMA: poly(N,N-dimethylacrylamide)) block polymer, it undergoes a microphase separation between the PNIPAm and PDMA phases, which is mainly resulted from the increased hydrogen bond strength [40]. Due to the microphase separation, experimental results [40] revealed that the shear elastic moduli of the PNIPAm-PDMA hydrogels were significantly increased from 0.96 kPa to 11.22 kPa with an increase in the temperature from 310 K to 329 K, whereas the shear loss moduli were increased from 0.076 kPa to 1.07 kPa. With the further increase in the degree of microphase separation, the moduli were increased significantly, thus resulting in an enhancement in the mechanical properties of the PNIPAm-PDMA block polymer [40]. However, so far, few

theoretical studies have been done to understand this coupling effect and explore the design principles for self-assembly of molecules.

In this study, a free-energy function is firstly formulated to describe the working principle of self-assembly for polymers during their microphase separation processes [27,41-43], based on the self-consistent field model [41,42]. A non-Euclidean geometry model, incorporating the thermodynamics of microphase separation, is proposed to understand the chemo-mechanical coupling between the chemical self-assembly and the mechanical elasticity, based on the non-Euclidean geometry equation [44] and rubber elasticity theory [45-47]. The non-Euclidean geometry parameters for a p-sided polygon and junction functionality (q) for the self-assembled networks, as well as radius (R_d) for microphases are applied and examined. Finally, effectiveness of the proposed model is verified using both finite-element analysis (FEA) and experimental results reported in literature.

2. Theoretical framework

2.1 Thermodynamics of microphase separation in self-assembly

As reported in Refs. [4,15-19,29,48,49], triblock PMMA-PDMS-PMMA polymer system has many advantages, i.e., good biocompatibility and mechanical performance. They have been found in jellyfish, iliac artery and muscle fiber [48]. They are non-toxic to human body and easily obtained [15-19,29,48,49]. They have highly designable mechanical properties with a modulus range from 3.4 to 77.4 kPa [15-19,29,48,49] and excellent mechanochromic and electrical properties [29,48,49], enabling it with great practical and potential applications.

As reported in Ref. [29], triblock PMMA-PDMS-PMMA polymer (in which PMMA: poly(methylmethacrylate) works as a bottlebrush backbone, and PDMS: polydimethylsiloxane acts as the bottlebrush side chain) can be synthesized via self-assembly of triblock copolymers. Experimental results [29] revealed that the size of PMMA microphases, which undergo separations with PDMS microphases, played an essential role to determine the mechanical property of PMMA-PDMS-PMMA polymers.

Based on a self-consistent field theory [41,42], the ordered free-energy (F_{ord}) is employed to describe the thermodynamics in microphase separation of polymers,

$$\begin{aligned}\frac{F_{\mathrm{ord}}}{N_c k_B T} &= F_{\mathrm{el}} + F_{\mathrm{int}} = -\ln \int dr q(r,s) \\ &+ \int dr[\chi N \phi_A \phi_B - \omega_A \phi_A - \omega_B \phi_B - \xi(1-\phi_A-\phi_B)]\end{aligned} \tag{1}$$

where F_{el} is the free energy of elasticity, F_{int} is the interfacial free energy, k_B=1.38×10^{-23} J/K is the Boltzmann constant, T is the temperature, N_c is the number of polymer chains, r is the position vector in interface, s is the degree of segment participation (s=1 if all segments are involved), ϕ_A and ϕ_B represent the distribution functions of components A and B in the block polymer, respectively. χ is the Flory-Huggins interaction parameter, 2N is the number of A and B segments in a polymer chain, and ξ is a pressure constant that ensures a local incompressibility [41,42]. $q(r,s)$ is the distribution function and represents the probability of segment participation degree (s) at position r.

The distribution function $q(r,s)$ is governed by the diffusion equation owing to mass conservation during the microphase separation [41-43],

$$\frac{\partial q(r,s)}{\partial s} = \frac{b^2}{6}\frac{\partial^2 q(r,s)}{\partial r^2} - \omega q(r,s) \tag{2}$$

where b is the length of a polymer segment. ω is either ω_A or ω_B, where ω_A and ω_B represent for the components A and B, respectively [41,42].

Here, non-coupling effect between the parameters of r and s has been considered, and it is expected that the degree of segment participation (s) has not been influenced by the position vector in interface (r). When the parameters of r and s are not linked with each other, equation (2) can be simplified as,

$$q(r,s) = q_r(r)q_s(s) \tag{3}$$

where $q_r(r)$ and $q_s(s)$ are the distribution functions related to r and s, respectively.

Due to the asymptotic rule of infinite polymerization, the solutions to the modified diffusion equation can be written as [42,43],

$$\phi_A = \frac{1}{2}[1+\tanh(-\sqrt{6\chi}\frac{r}{b})] \tag{4a}$$

$$q_{rA}(r) = [1+\exp(-2\sqrt{6\chi}\frac{r}{b})]^{-1/2} \tag{4b}$$

$$\phi_B = \frac{1}{2}[1+\tanh(\sqrt{6\chi}\frac{r}{b})] \tag{5a}$$

$$q_{rB}(r) = [1+\exp(2\sqrt{6\chi}\frac{r}{b})]^{-1/2} \tag{5b}$$

$$q_s(s) = \exp(-\xi_0 s) \tag{6}$$

$$\begin{cases} \omega_A = \chi N\phi_B + \xi \\ \omega_B = \chi N\phi_A + \xi \end{cases} \tag{7}$$

where q_{rA} and q_{rB} are the distribution functions of components A and B, respectively. ξ_0 is the initial pressure and ξ is the local incompressibility.

Substituting equation (7) into (1), the ordered free energy of polymers can be rewritten as,

$$\frac{F_{ord}}{N_c k_B T} = -\ln \int dr q(r,s) - \int (\chi N \phi_A \phi_B + \xi) dr \tag{8}$$

If the volume change of microphase separation is very small, i.e., $\xi \approx 0$ [42,43], the ordered free energy can be expressed as,

$$\frac{F_{ord}}{N_c k_B T} = \xi_0 s - \ln \int dr q_{rA}(r) - \int \chi N \phi_A \phi_B dr \tag{9}$$

According to the continuum mechanics [20,21], the vector *r* presents the end-to-end distance of a polymer chain, which can be described by the elongation ratio λ as,

$$\begin{cases} r = \sqrt{\dfrac{\lambda_1^2 + \lambda_2^2 + \lambda_3^2}{3}} r_0 \\ \dfrac{\partial r}{\partial \lambda} = \dfrac{\lambda - 1/\lambda^2}{\sqrt{3\lambda^2 + 6/\lambda}} r_0 \left(\lambda_1 = \lambda \ \text{ and } \ \lambda_2 = \lambda_3 = \lambda^{-1/2} \right) \end{cases} \tag{10}$$

where λ_1, λ_2 and λ_3 represent the elongation ratios along three directions. r_0 is initial position vector. The relationships of $\lambda_1=\lambda$ and $\lambda_2=\lambda_3=\lambda^{-1/2}$ are used for the uniaxial tensile stretching, and the volume invariance of isotropic polymer is $\lambda_1\lambda_2\lambda_3=1$.

Combining equations (9) and (10), the constitutive relationship of true stress (σ) as a function of elongation ratio (λ) can be obtained as,

$$\begin{aligned} \frac{\sigma}{N_c k_B T} &= \lambda \frac{\partial F_{ord} / \partial \lambda}{N_c k_B T} = \{ p_h - [1 + \exp(-2\sqrt{6\chi}\, \frac{r}{b})]^{-1/2} \\ &- \frac{\chi N}{4} [1 + \tanh(-\sqrt{6\chi}\, \frac{r}{b}) \tanh(\sqrt{6\chi}\, \frac{r}{b})] \} \lambda \frac{\partial r}{\partial \lambda} \end{aligned} \tag{11}$$

where p_h is the hydrostatic pressure and $\int_0^{r_0} q_{rA} dr \approx 1$, if the length of chain is infinite [41-43].

To verify the effectiveness of equation (11), true stresses of self-assembled polymers undergoing microphase separations as a function of elongation ratio are obtained using FEA simulations. The obtained results are plotted in Figure 1, where the microphase separation undergoes a non-Euclidean geometry transition from spheroid (coin) to cylinder (lamellar). Here, the Poisson's ratio of the polymer is chosen as 0.45 [45-47]. The radii of all four coin-shaped phases are 2 mm, as shown in Figure 1(b). The width and length of lamellar/cylindrical phase are 2.5 mm and 20 mm, whereas the area of the four coins is equal to that of the lamellar vertical strip. The 8-node hexahedron element, C3D8R, is used to perform the FEA. 8000 elements are used to model the unit with a size of 20×20 mm^2, as shown in Figures 1(a), 1(b) and 1(c). The moduli of the homogenous polymer and microphase separation inclusion are chosen as 1 MPa and 2 MPa, respectively. Figure 1(d) shows the FEA simulation results, which reveal that the stresses reach their maximum values of 0.50 MPa, 0.54 MPa to 0.57 MPa for the homogeneous, coin shaped and cylindrical/strip microphase separations, and their strain energy values are increased from 0.100 J, 0.108 J to 0.113 J. These analytical results clearly indicate that the morphology of microphase separation influences the mechanical performance of the polymer. Given the same volume fraction (e.g., $4\times\pi\times2^2$ mm$^2\approx2.5\times20$ mm^2), mechanical optimization may occur owing to different geometries of microphase separations in polymer.

Moreover, as can be seen from the curves shown in Figure 1(e), different volume fractions (i.e., the number of spheres) of microphases in the self-assembled polymer have been compared with the FEA results as presented in Figure 1(f). The stresses

reach their maximum values of 0.50 MPa, 0.52 MPa, 0.54 MPa, 0.56 MPa to 0.59 MPa for the number of spheres of 0, 2, 4, 6 and 8 (with their corresponding volume fractions of 0%, 6.28%, 12.56%, 18.85% and 25.13%), respectively. These analytical results support that the volume fraction of microphase significantly influences the mechanical performance of self-assembled polymer. With an increase in the contents of self-assembled molecules, the volume fraction of microphase is then increased in the polymer, of which the mechanical property is therefore reinforced.

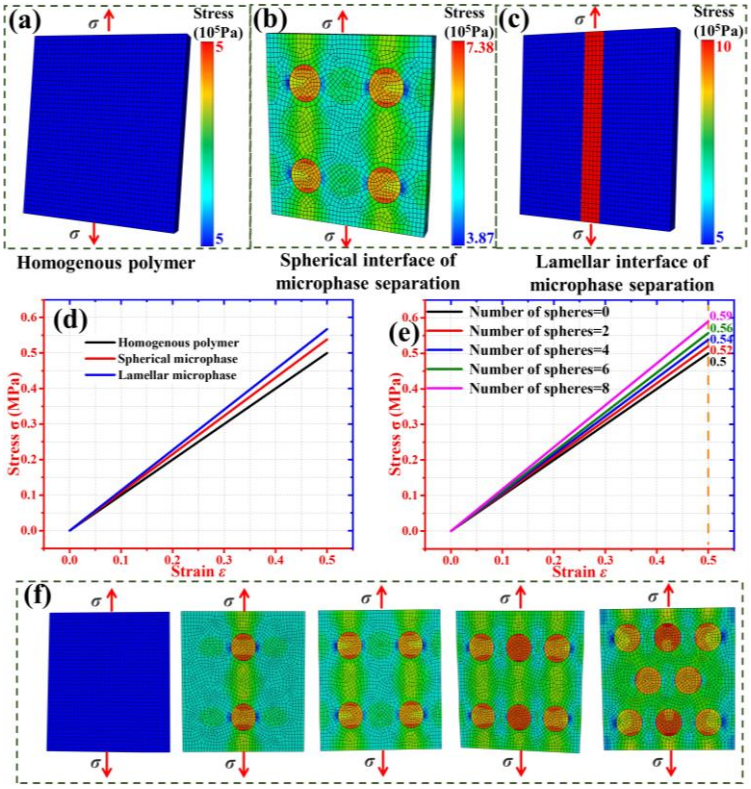

Figure 1. Finite-element analysis of stress-strain in the polymer with coin shaped and lamellar microphases. (a) For homogenous polymer without microphase separation. (b) For polymer with coin shaped interface of microphase separation. (c) For polymer with lamellar interfaces of microphase separation. (d) Resultant stress-strain curves. (e) The stress-strain of different volume fraction (i.e., 0, 6.28%, 12.56%, 18.85% and 25.13%) of microphase in self-assembled polymer. (f) FEA simulations of different volume fractions of microphases self-assembled polymer.

2.2 Non-Euclidean geometry model of microphase separation

Microphase separation is determined by the cross-linked networks [44-47], which are originated from the self-assembly of the molecules in the polymer. It can be found that only regular triangles, regular quadrilaterals and regular hexagons are chosen to fill into the space. However in fact, there must be a lot of defects in the network, and pentagons (p-sided polygon) are also widespread, which is not a single unit to form a network. In the real polymer network [45-47], these objective factors all lead to the formation of the network chains in a non-Euclidean geometry way, which is due to the large cross-linking junction functionality (q) of the network self-assembly, and the aggregation of multiple units at a cross-linking point will trigger the non-planar nature of the network. The non-Euclidean geometric properties of the network are described by the tangent circle radius (R_d) of the surface. The larger the area of the in plane polygon (A_r) is, the fewer the irregular patterns and the flatter the plane will be. Therefore, it is necessary to employ the non-Euclidean geometry model [44] to describe the self-assembled networks, and then to formulate their microphase separations. Figure 2 show four types of such hypothesized self-assembled networks with chains emanating from cross-linking points. These chains have the same length and form a p-sided polygons.

In a regular polygon, the number of chains (N_c) is proportional to $p\times2\tan(180°/p)/p$, and the area of regular polygon is proportional to $p/[4\tan(180°/p)]$. As can be seen from the p-sided regular polygon shown in Figure 2, it can be divided into p isosceles triangles with a vertex angles of $360°/p$. The area of p-sided regular polygon is

considered as that of p isosceles triangles, e.g., p/[4tan(180°/p)]. When the area of the network is kept a constant, the number of chains (N_c) can be then obtained, i.e., p×2tan(180°/p)/p. According to the rubber elasticity theory [47], the number of chain (N_c) plays a critical role to determine the mechanical elasticity property of the polymer. FEA simulation is carried out to study the effect of regular polygons on the mechanical performance under a constant strain of 50%. Here, the applied FEA model and design method are the same with the previous ones. The Poisson's ratio and modulus of the polymer are chosen as 0.45 and 1 MPa, respectively. The 8-node hexahedron element, C3D8R, is used to perform the FEA simulation. 8000 elements are used to model the unit with a size of 20×20 mm^2 and the width of each line is 1 mm. In a 20×20 mm^2 cell, the chain lengths of all four types of regular polygons are assumed to be 10 mm. Poisson's ratios and moduli of all chains are chosen as 0.45 and 1 MPa, respectively.

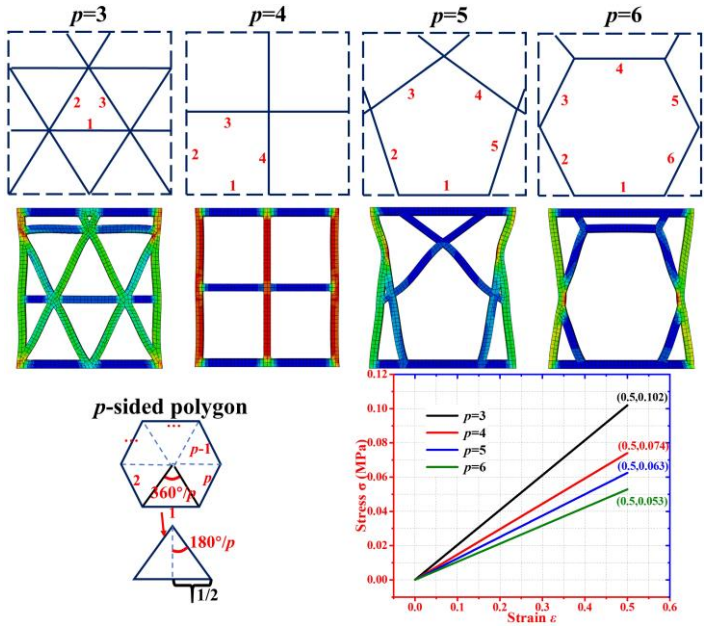

Figure 2. Schematic illustrations of self-assembled networks by non-Euclidean geometry in terms of p-sided polygons and their stress-strain curves.

The simulation results show that the strain energy values are decreased from 10.6×10^{-3} J, 7.7×10^{-3} J, 6.5×10^{-3} J to 5.5×10^{-3} J with an increase of the p values from 3, 4, 5 to 6 for the p-sided polygons, and the stress is decreased from 0.102 MPa, 0.074 MPa, 0.063 MPa to 0.053 MPa (at the same strain of ε=0.5 and the stress was reduced by 48%), with an increase in the p values from 3, 4, 5 to 6 for the p-sided polygon, respectively. Due to the same length of polymer chain, the triangle polygon has 6 complete units, the square polygon has 4 complete units, whereas the pentagon and hexagon ones have only one complete unit. According to the rubber elastic theory [45-47], the crosslinking density per volume is decreased with the increase of p, thus causing the decreases of both strain energy and stress. On the other hand, effect of junction functionality (q) on the p-sided polygon is investigated, and the obtained results are shown in Figure 3. In this case, the non-Euclidean geometry equation can be written as $1/R_d=-p\pi(1-2/p-2/q)/A_r$, where R_d is the radius of ellipsoid (or spheroid) and A_r is the area of polygon [44].

The first row of Figure 3 shows the effect of junction functionality (q) on the self-assembled polymer network, of which the geometry is described using the increased number of self-assembled molecule chains. The second row shows the effect of junction functionality (q) on self-assembled polymer network, of which the non-Euclidean geometry will be gradually increased with an increase in the junction functionality (q). The third row shows the effects of junction functionality (q) and R_d on self-assembled polymer network, of which the non-Euclidean geometry will be gradually increased with increases in the junction functionality (q) and R_d. The fourth

row shows the effect of junction functionality (q) on microphase, in which the non-Euclidean geometry is increased with increases in q and R_d, resulting in an ellipsoid shape. The areas of spheroid and ellipsoid are kept constants during simulations, i.e., $\pi\times2\times2$ mm^2 and $\pi\times1\times4$ mm^2, respectively. The simulation results show that the strain energies are 0.112 J and 0.115 J for the spheroid and ellipsoid microphases, respectively. These simulation results support that the transition between spheroid and ellipsoid microphases is determined by the junction functionality (q), which plays a critical role to determine the strain energy. Therefore, the constitutive relationship between the microphase separation and non-Euclidean geometry equation should be investigated.

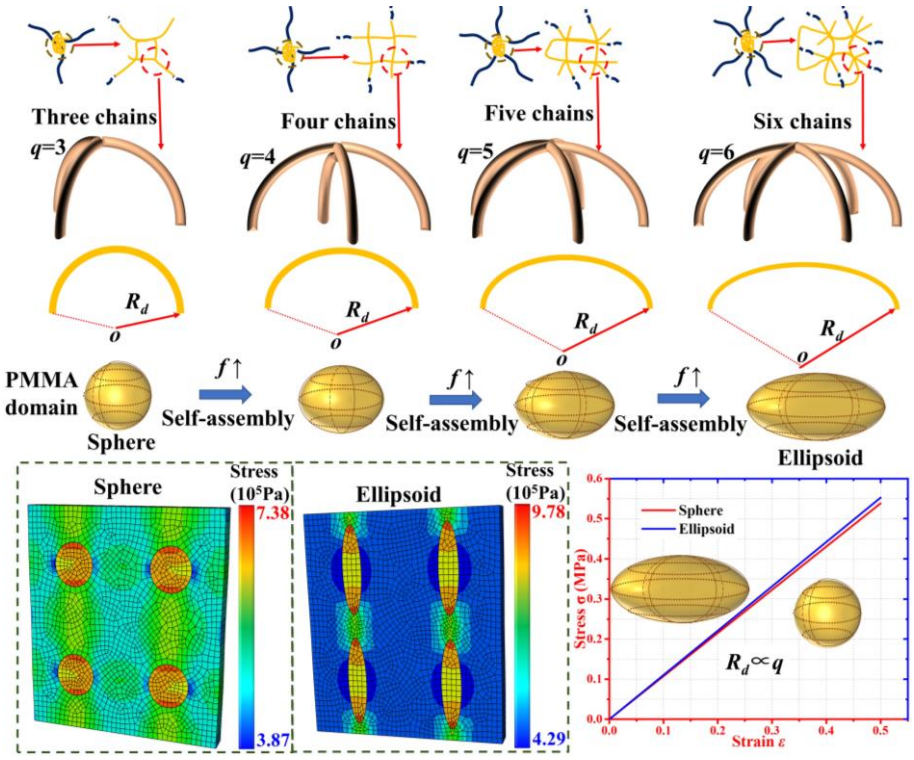

Figure 3. Schematic illustrations of self-assembled networks and spheroid/ellipsoid microphase by junction functionality (q) and the ellipsoid radius (R_d), where q and R_d are ruled by the non-Euclidean geometry equation of $1/R_d=-p\pi(1-2/p-2/q)/A_r$.

One advantage of using the non-Euclidean geometry to simulate the polymer network is that it provides a geometrical manner to characterize the microphase separation and simulate the mechanical properties by *p*-side polygons and junction functionality (*q*) using FEA analysis. Furthermore, the mathematical equation can be used to describe the chemo-mechanical coupling in the self-assembled polymers in terms of geometrical shape transition of polymer network. Another advantage of the non-Euclidean geometry is to describe the microphase, of which the morphological transition is originated from the self-assembly of polymer network and the externally mechanical loading.

Here, the rubber elastic theory [45,46] and phantom model [46,47] have been introduced to explore the constitutive relationship of non-Euclidean geometry parameters and elasticity of the self-assembled network. Combining equations (10) and (11), the true stress as a function of elongation ratio can be written as,

$$\sigma = 2(1-\frac{2}{q})\tan\frac{180^\circ}{p} N_c k_B T\{p_h - [1+\exp(-2\sqrt{6\chi}\,\frac{r}{b})]^{-1/2} - \frac{\chi N}{4}[1+\tanh(-\sqrt{6\chi}\,\frac{r}{b})\tanh(\sqrt{6\chi}\,\frac{r}{b})]\}\lambda\frac{\partial r}{\partial\lambda} \tag{12a}$$

$$r = \sqrt{\frac{\lambda^2+2/\lambda}{3}}r_0 \quad \text{and} \quad \frac{\partial r}{\partial\lambda} = \frac{\lambda-1/\lambda^2}{\sqrt{3\lambda^2+6/\lambda}}r_0 \tag{12b}$$

To verify the equation (12), analytical results of the proposed model are obtained and plotted in Figure 4, in which the non-Euclidean geometry of *p*-sided polygon network and junction functionality (*q*) are varied. Parameters used in the equation (12) for calculations of these values are p_h=3.4, q=4, χ=0.11, r_0=0.2b, N=100 and $N_c k_B T$=0.2 MPa for Figure 4(a); p_h=3.4, p=4, χ=0.11, r_0=0.2b, N=100 and $N_c k_B T$=0.2

MPa for Figure 4(b). Results show that the stress is decreased from 5.79 MPa to 1.61 MPa at the same elongation ratio of λ=6, with an increase in the p from 3 to 7. Based on the rubber elastic theory [45-47], the cross-linking density is gradually decreased with an increase in the non-Euclidean geometry of p-sided polygons, thus resulting in a decreased stress.

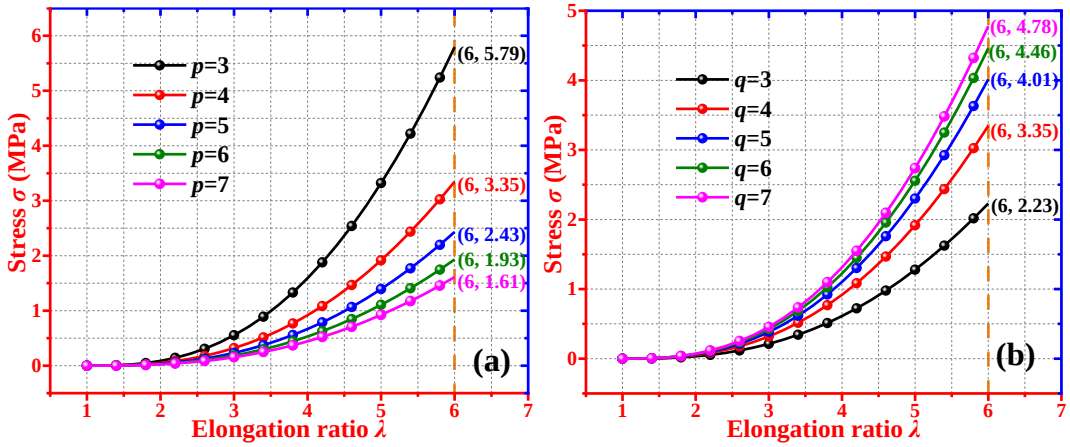

Figure 4. Analytical results of equation (12) for the effects of non-Euclidean geometries on the stress-elongation ratio behaviors. (a) Effect of non-Euclidean geometry of p-sided polygon network on the stress-elongation ratio behavior, where p=3, 4, 5, 6 and 7. (b) Effect of non-Euclidean geometry of junction functionality (q) on the stress-elongation ratio behavior, where q=3, 4, 5, 6 and 7.

Analytical results of the effects of non-Euclidean geometry of junction functionality (q) on stress-elongation ratio are plotted in Figure 4(b). With an increase in the junction functionality (q) from 3, 4, 5, 6 to 7, the stress is gradually increased from 2.23 MPa, 3.35 MPa, 4.01 MPa, 4.46 MPa to 4.78 MPa at the same elongation ratio of λ=6. These analytical results can also be explained by the rubber elasticity theory [45-47]. With an increase in the junction functionality (q), the cross-linking

density is increased in the self-assembled network, thus causing the increases of both stress and elasticity at the same elongation ratio.

3. Experimental verification

Experimental data reported in Refs. [29,48,49] for the triblock PMMA-PDMS-PMMA polymers are used to verify the analytical results generated from the proposed model. Levenberg-Marquardt optimization algorithm is adopted for all the calculation parameters. The corresponding termination condition is that the value of residual sum of squares does not decay for at least 100 times, at a given p=4 and q=6 based on the rubber elasticity theory [45-47]. Here, N_c is the number of chains, k_B=1.38×10^{-23} J/K is the Boltzmann constant, T≈298.15 K is temperature, p_h is the hydrostatic pressure which is used for the initial boundary condition, 2N≈2000 is the number of A and B segments in a copolymer chain [28,48,49], b≈1 nm is the length of a segment [41-46], r_0≈0.15 nm is the initial position vector which is similar to the length of covalent bonds [41-43]. For the PMMA-PDMS-PMMA system of self-assembled block copolymer with the microphase separation. χ, the Flory-Huggins interaction parameter can be estimated being less than 0.2 [45,46]. This results in that the range of $\sqrt{\chi}\frac{r_0}{b}$ is from 0 to 0.07, and χN is ranged from 10.5 to 200 [41-43]. Here the $N_c k_B T$ is used for the modulus of polymer network [47]. These parameters are determined by the experimental results, and can be well fitted using the existing experimental data reported in literature. In order to obtain a realistic network structure, we have checked the reported experimental results [29,48,49]. These papers reported that the non-Euclidean geometry [44] can simultaneously characterize the deformation

characteristics of 3-sided and 4-sided polygon networks, and therefore based on these references, q=6 is selected.

To experimentally verify the proposed model of equation (12), the analytical results have been obtained and then plotted to predict the relationship between mechanical stress-elongation ratio of the PMMA-PDMS-PMMA polymers [29]. The effects of volume fraction of PMMA (f) have been investigated and the results with the same number of PDMS segment (N_B) are shown in Figure 5. The analytical results of classical Mooney-Rivlin (M-R) model ($\sigma=(2C_1+2C_2/\lambda)(\lambda-1/\lambda^2)$, where C_1 and C_2 are material constants [46,47], are also plotted for comparisons. All the parameters used in the equation (12) are listed in Table 1. With an increase in the PMMA volume fraction from f=0.07, f=0.09 to f=0.16, the maximum stress is increased from 2.06×10^5 Pa, 3.78×10^5 Pa to 3.88×10^5 Pa as shown in Figure 5(a). It is revealed that the analytical results obtained from the proposed model are close to the experimental results, in comparison with those obtained from of the M-R model [46,47]. In Figure 5(b), the correlation index R^2 between analytical and experimental results are calculated to be 98.28%, 99.77% and 99.48% for the PMMA-PDMS-PMMA polymers of f=0.07, f=0.09 and f=0.16, respectively. It can be clearly seen that the analytical results agree well with the experimental data ($|\Delta\sigma|<0.25\times10^5$ Pa).

Table 1. Values of parameters used in equation (12) for PMMA-PDMS-PMMA polymer.

f	$N_c k_B T$ (10^5Pa)	p_h	χN	C_1 (10^5Pa)	C_2 (10^5Pa)	$\sqrt{\chi}\frac{r_0}{b}$
0.07	1.91	17.25	64.48	0.17	-0.31	0.035
0.09	3.06	19.48	73.36	0.31	-0.52	
0.16	4.41	27.57	106.08	0.51	-0.84	

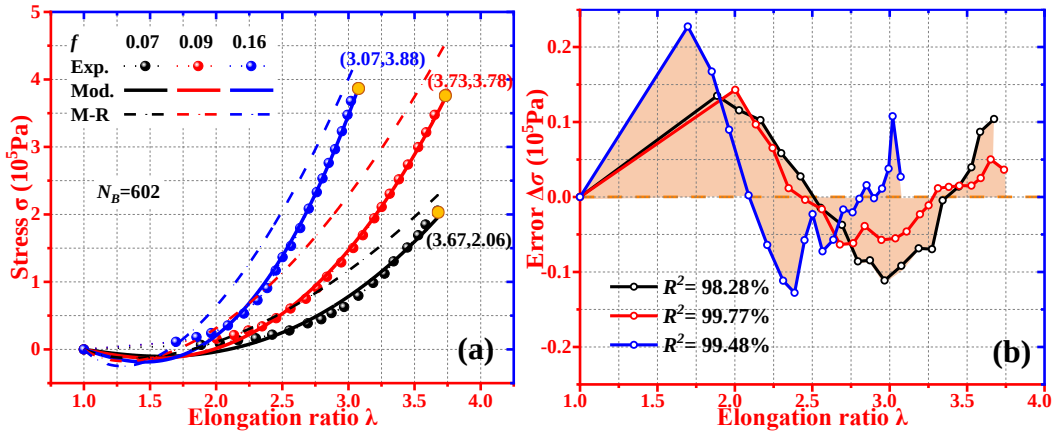

Figure 5. Effect of PMMA volume fraction (f) on the mechanical stress-elongation ratio behavior of PMMA-PDMS-PMMA polymer, where f=0.07, f=0.09 and f=0.16. (a) Comparisons among analytical results using equation (12), M-R model [46,47] and experimental data [29] for PMMA-PDMS-PMMA polymers. (b) Divergences of analytical and experimental results of stress.

Furthermore, analytical results of stress-elongation ratio obtained using the equation (12) are plotted in Figure 6(a), which has also included the experimental data of PMMA-PDMS-PMMA polymers with various volume fractions (f) of PMMA reported in Ref. [48]. All the parameters used in the equation (12) are listed in Table 2.

Table 2. Values of parameters used in equation (12) for PMMA-PDMS-PMMA triblock polymer.

f	$N_c k_B T(10^5$ Pa)	p_h	χN	$\sqrt{\chi}\frac{r_0}{b}$
0.03	0.75	4.01	10.83	0.049
0.11	2.98	18.14	68.36	
0.14	4.12	17.29	64.84	

Both the analytical and experimental results show that the stress of PMMA-PDMS-PMMA polymer is significantly increased from 0.04×10^5 Pa, 0.48×10^5 Pa to 0.72×10^5 Pa at the same elongation ratio of λ=2, with an increase

in the volume fraction of PMMA (f) from 0.03, 0.11 to 0.14. The analytical curves fit well with those from the experimental data. On the other hand, the divergences between the analytical and experimental results are calculated using the correlation index (R^2), which are 99.12%, 98.93% and 99.14% for f=0.03, f=0.11 and f=0.14, respectively, as shown in Figure 6(b).

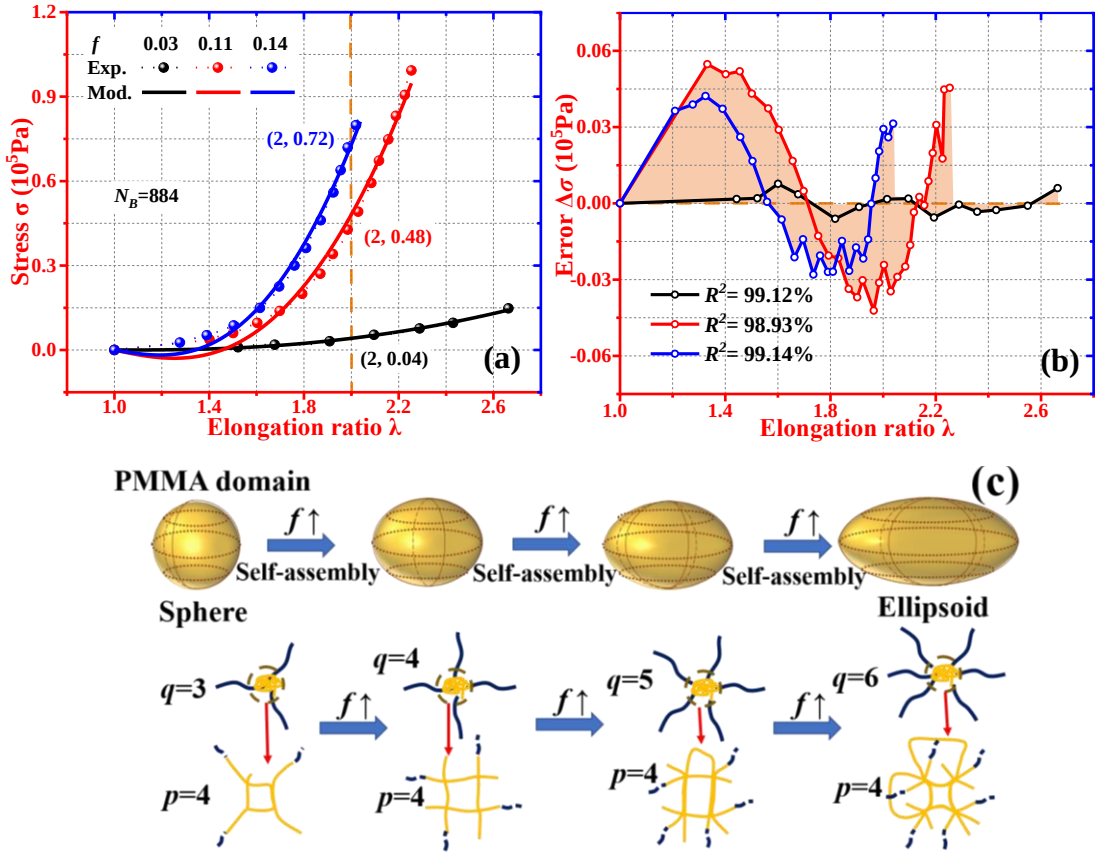

Figure 6. Analytical results from current model and experimental data [48] of mechanical stress-elongation ratio behaviors of PMMA-PDMS-PMMA polymers, at given N_B=884 and various PMMA volume fraction (f) of 0.03, 0.11 and 0.14. (a) The stress-elongation ratio curves. (b) Divergences of analytical and experimental results of stress. (c) Schematic illustration of the morphology transformation of microphase separation with respect to non-Euclidean geometry of junction functionality (q).

Figure 6(c) illustrates the working principle of the effect of PMMA volume fraction on microphase separation in the PMMA-PDMS-PMMA polymer. With an increase in the PMMA volume fraction, the junction functionality (q) is increased, resulting in the microphase separation, of which the morphology is transformed from spheroid to ellipsoid. According to the thermodynamics of microphase separation, the stiffness of the self-assembled polymer is therefore enhanced with an increase in the junction functionality (q).

To verify the effect of segment number of PMMA on the mechanical behavior, equation (12) is applied to predict the mechanical stress-elongation ratio of PMMA-PDMS-PMMA polymer [49]. The obtained results are shown in Figure 7(a) for the polymers with various numbers of PMMA segment of N_A=200, 300, 700 and 1200. Values of parameters used in equation (12) in the calculations are listed in Table 3. With the increased numbers of PMMA segments (N_A) from 300, 700 to 1200, the stress of the PMMA-PDMS-PMMA polymer is increased from 0.68×10^5 Pa, 1.23×10^5 Pa to 3.57×10^5 Pa at the same elongation ratio of λ=3. Meanwhile, the divergences between the analytical and experimental results have been calculated based on correlation index (R^2), which are 98.55%, 99.90%, 99.89% and 98.05% for the numbers of PMMA segment of N_A=200, 300, 700 and 1200, respectively, as shown in Figure 7(b). Figure 7(c) shows the working principles of the effect of PMMA segment length on microphase separation. The stress of the polymer is enhanced with an increase in the number of PMMA segment, which increases the non-Euclidean

geometry of junction functionality (q), causing the morphology of microphase transformed from the spheroid one into the ellipsoid one.

Table 3. Values of parameters used in equation (12) for PMMA-PDMS-PMMA polymer.

N_A	$N_c k_B T(10^5\,\mathrm{Pa})$	p_h	χN	$\sqrt{\chi}\frac{r_0}{b}$
200	0.65	18.98	73.12	0.056
300	1.29	19.74	76.55	
700	2.17	22.11	85.32	
1200	6.82	20.54	78.04	

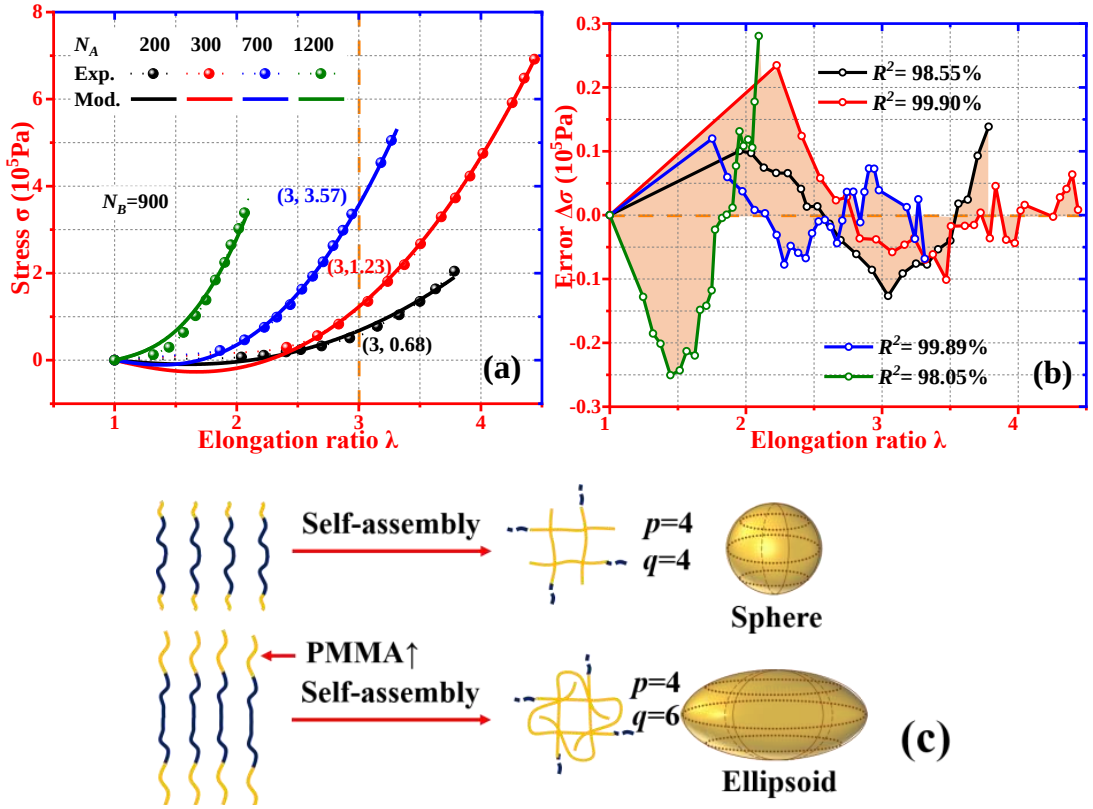

Figure 7. Analytical results from equation 12 and experimental data [49] of mechanical stress-elongation ratios of PMMA-PDMS-PMMA polymers, at given N_B=900 and various numbers of PMMA segment of N_A=200, 300, 700 and 1200. (a) The stress-elongation ratio curves. (b) Divergences of analytical and experimental results of stress. (c) Schematic illustration of the morphology of microphase by non-Euclidean geometry of junction functionality (q).

Furthermore, effects of volume fraction (f) of PMMA on the mechanical stress-elongation ratios of PMMA-PDMS-PMMA polymer have been evaluated and the obtained data are plotted in Figure 8(a). All the parameters used in the equation (12) are listed in Table 4. With an increase in the PMMA volume fraction from f=0.03, 0.06, 0.11 to 0.19, the stress is increased from 0.17×10^5 Pa, 0.17×10^5 Pa, 0.37×10^5 Pa to 2.99×10^5 Pa at the same elongation ratio of λ=2. These analytical results fit well with the experimental data [29] of PMMA-PDMS-PMMA polymers with an error $|\Delta\sigma|<0.2\times10^5$ Pa, as shown in Figure 8(b). The divergences between the analytical and experimental results have been compared based on the data of correlation index (R^2), which are R^2=98.66%, 99.94%, 99.69% and 99.08% for f=0.03, 0.06, 0.11 and 0.19, respectively. Figure 8(c) illustrates the working principle for the increased PMMA volume fraction on the mechanical stress-elongation behavior of PMMA-PDMS-PMMA polymers. Results show that the length of PMMA chain is gradually increased with an increase in the PMMA volume fraction in the PMMA-PDMS-PMMA polymer. Based on the thermodynamics in microphase separation, the PMMA chain length determines the interfacial thickness (r_0N) of the microphase separation, resulting in the increase of both the radius ($1/R_d=-p\pi(1-2/p-2/q)/A_r$) of ellipsoid (or spheroid) and strain energy. Therefore, a larger mechanical stress is then needed at the same elongation ratio.

In this study, both the free energy of elasticity (F_{el}) and interfacial free energy (F_{int}) are employed to formulate the thermodynamics of microphase separation. However, the interfacial free energy (F_{int}) shows a much larger error at the low elongation ratios,

because the interface between microphase and matrix has not been involved to resist to the external loading. Thus, the mechanical energy is lost because the interfacial free energy (F_{int}) shows high errors at low elongation ratios in Figure 5 to Figure 8.

Table 4. Values of parameters used in equation (12) for PMMA-PDMS-PMMA polymer.

f	$N_c k_B T(10^5\,\text{Pa})$	p_h	χN	$\sqrt{\chi}\frac{r_0}{b}$
0.03	1.05	20.45	78.28	0.044
0.06	1.65	24.09	93.12	
0.11	2.40	29.98	116.24	
0.19	7.17	35.01	135.99	

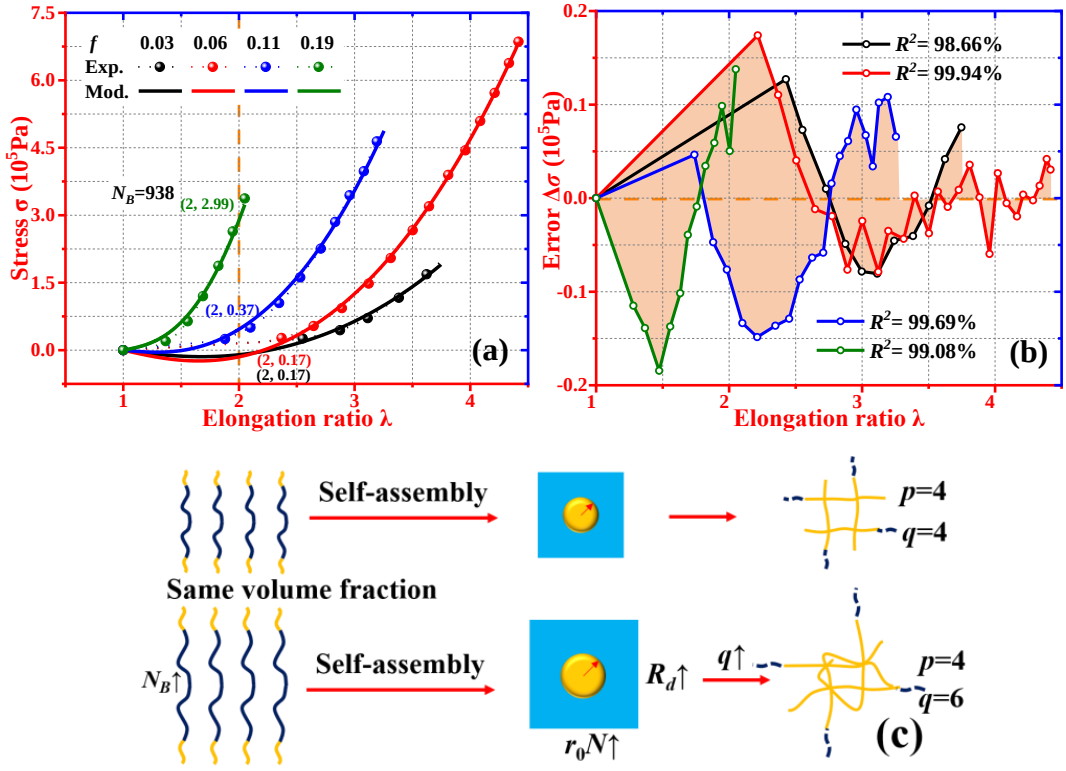

Figure 8. Analytical and experimental results [29] of the stress-elongation ratio, at given N_B=938 and various PMMA volume fraction of f=0.03, 0.06, 0.11 and 0.19. (a) The stress-elongation ratio curves. (b) Divergences of analytical and experimental results of stress. (c) Schematic illustration of the effect of PMMA volume fraction on microphase separation by the non-Euclidean geometry of ellipsoid radius (R_d).

4. Conclusions

A new non-Euclidean geometry model is proposed to represent the mechanics of the chemo-mechanical coupling in the self-assembled polymer. The geometrical parameters, p-sided polygons and junction functionality (q), are applied to estimate the mechanical elasticity of self-assembled and cross-linked network. Meanwhile, the radius (R_d) of microphase is also characterized using the geometrical parameters of p and q, to describe the thermodynamic microphase separation and morphology transformation. This non-Euclidean geometry framework is able to combine with the chemical self-assembly of microphase separation and mechanical elasticity of cross-linked network, to explore the working principle of chemo-mechanical coupling in self-assembled polymer. The geometrical parameters of p and q are helpful to characterize the rubber elasticity of polymer network, which is originated from the self-assembly of molecule chains and determined by the thermodynamics of microphase separation. Therefore, the proposed model provides a fundamental approach to explore the working principle in self-assembly, in combination of rubber elasticity theory and thermodynamics of microphase separation. However, it should be noted that the non-Euclidean geometry morphology and its transformation should be formulated for the constitutive relationship of microphase separation and mechanical property of self-assembled polymer systems.

Conflicts of interest

There are no conflicts to declare.

Acknowledgements

This work is supported by National Natural Science Foundation of China (NSFC) under Grant No. 11725208 and 12172107, and the Newton Mobility Grant (IE161019) through the UK Royal Society and NFSC.

References

[1] M. Nguyen, Y. Qiu, S. Vaikuntanathan, Organization and self-assembly away from equilibrium: toward thermodynamic design principles, Annu. Rev. Condens. Matter Phys. 12 (2021) 273-290.

[2] A.M. Rumyantsev, N.E. Jackson, J.J. de Pablo, Polyelectrolyte complex coacervates: recent developments and new frontiers, Annu. Rev. Condens. Matter Phys. 12 (2021) 155-176.

[3] M. Driscoll, B. Delmotte, M. Youssef, S. Sacanna, A. Donev, P. Chaikin, Unstable fronts and motile structures formed by microrollers, Nat. Phys. 13 (2017) 375-379.

[4] M. Vatankhah-Varnosfaderani, W.F.M. Daniel, M.H. Everhart, A.A. Pandya, H. Liang, K. Matyjaszewski, A.V. Dobrynin, S.S. Sheiko, Mimicking biological stress–strain behaviour with synthetic elastomers, Nature 549 (2017) 497-501.

[5] G.S. Georgiev, E.B. Kamenska, E.D. Vassileva, I.P. Kamenova, V.T. Georgieva, S.B. Iliev, I.A. Ivanov, Self-assembly, antipolyelectrolyte effect, and nonbiofouling properties of polyzwitterions, Biomacromolecules 7 (2006) 1329-1334.

[6] J.H. Fendler, Chemical self-assembly for electronic applications, Chem. Mater. 13 (2001) 3196-3210.

[7] J.H. Lee, C.Y. Koh, J.P. Singer, S.J. Jeon, M. Maldovan, O. Stein, E.L. Thomas, 25th Anniversary article: ordered polymer structures for the engineering of photons and phonons, Adv. Mater. 26 (2014) 532-569.

[8] D. Zhang, T.K. Ronson, J.R. Nitschke, Functional capsules via subcomponent self-assembly, Accounts Chem. Res. 51 (2018) 2423-2436.

[9] T. Matsuda, T. Nakajima, J.P. Gong, Fabrication of tough and stretchable hybrid double-network elastomers using ionic dissociation of polyelectrolyte in nonaqueous media, Chem. Mater. 31 (2019) 3766-3776.

[10] B.A.K. Kriebisch, A. Jussupow, A.M. Bergmann, F. Kohler, H. Dietz, V.R.I. Kaila, J. Boekhoven, Reciprocal coupling in chemically fueled assembly: a reaction cycle regulates self-assembly and vice versa, J. Am. Chem. Soc. 142 (2020) 20837-20844.

[11] J. Zhan, Y. Cai, S. He, L. Wang, Z. Yan, Tandem molecular self-assembly in liver cancer cells, Angew. Chem. Int. Ed. 130 (2017) 1831-1834.

[12] K. Ariga, X. Jia, J. Song, J.P. Hill, D.T. Leong, Y. Jia, J. Li, Nanoarchitectonics beyond self-assembly: challenges to create bio-like hierarchic organization, Angew. Chem. Int. Ed. 59 (2020) 15424-15446.

[13] J. Song, C. Yuan, T. Jiao, R. Xing, M. Yang, D.J. Adams, X. Yan, Multifunctional antimicrobial biometallohydrogels based on amino acid coordinated self-assembly, Small 16 (2020) 1907309.

[14] K. Ariga, T. Mori, T. Kitao, T. Uemura, Supramolecular chiral nanoarchitectonics, Adv. Mater. 32 (2020) 1905657.

[15] M. Jacobs, H. Liang, E. Dashtimoghadam, B.J. Morgan, S.S. Sheiko, A.V. Dobrynin, Nonlinear elasticity and swelling of comb and bottlebrush networks, Macromolecules 52 (2019) 5095-5101.

[16] H. Liang, Z. Wang, A.V. Dobrynin, Strain-adaptive self-assembled networks of linear-bottlebrush-linear copolymers, Macromolecules 52 (2019) 8617-8624.

[17] C. Clair, A. Lallam, M. Rosenthal, M. Sztucki, M. Vatankhah-Varnosfaderani, A.N. Keith, Y. Cong, H. Liang, A.V. Dobrynin, S.S. Sheiko, D.A. Ivanov, Strained bottlebrushes in super-soft physical networks, ACS Macro Lett. 8 (2019) 530-534.

[18] H.Y. Liang, G.S. Grest, A.V. Dobrynin, Brush-like polymers and entanglements: from linear chains to filaments, ACS Macro Lett. 8 (2019) 1328-1333.

[19] A.N. Keith, M. Vatankhah-Varnosfaderani, C. Clair, F. Fahimipour, E. Dashtimoghadam, A. Lallam, M. Sztucki, D.A. Ivanov, H.Y. Liang, A.V. Dobrynin, S.S. Sheiko, Bottlebrush bridge between soft gels and firm tissues, ACS Central Sci. 6 (2020) 413-419.

[20] D. Zhong, Y. Xiang, J. Liu, Z. Chen, H. Zhou, H. Yu, S. Qu, W. Yang, A constitutive model for multi network elastomers pre-stretched by swelling, Extreme Mech. Lett. 40 (2020) 100926.

[21] Y.H. Xiang, D.M. Zhong, P. Wang, T.H. Yin, H.F. Zhou, H.H. Yu, C. Baliga, S.X. Qu, W. Yang, A physically based visco-hyperelastic constitutive model for soft materials, J. Mech. Phys. Solids 128 (2019) 208-218.

[22] Z.Y. Xing, H.B. Lu, M. Hossain, Y.Q. Fu, J.S. Leng, S.Y. Du, Cooperative dynamics of heuristic swelling and inhibitive micellization in double-network hydrogels by ionic dissociation of polyelectrolyte, Polymer 186 (2020) 122039.

[23] Z.Y. Xing, H.B. Lu, Y.Q. Fu, Anchoring-mediated topology signature of self-assembled elastomers undergoing mechanochromic coupling/decoupling, Soft Matter 17 (2021) 5960-5968.

[24] L. Chen, T.L. Sun, K.P. Cui, D.R. King, T. Kurokawa, Y. Saruwatari, J.P. Gong, Facile synthesis of novel elastomers with tunable dynamics for toughness, self-healing and adhesion, J. Mater. Chem. A 7 (2019) 17334-17344.

[25] X.H. Zhao, Designing toughness and strength for soft materials, Proc. Natl. Acad. Sci. USA 114 (2017) 8138-8140.

[26] M. Nguyen, S. Vaikuntanathan, Design principles for non-equilibrium self-assembly, Proc. Natl. Acad. Sci. USA 113 (2016) 14231-14236.

[27] C.M. Bates, F.S. Bates, 50th Anniversary perspective: block polymers-pure potential, Macromolecules 50 (2017) 3-22.

[28] W. Yang, V.R. Sherman, B. Gludovatz, E. Schaible, P. Stewart, R.O. Ritchie, M.A. Meyers, On the tear resistance of skin, Nat. Commun. 6 (2015) 6649.

[29] M. Vatankhah-Varnosfaderani, A.N. Keith, Y. Cong, H.Y. Liang, M. Rosenthal, M. Sztucki, C. Clair, S. Magonov, D.A. Ivanov, A.V. Dobrynin, S.S. Sheiko,

Chameleon-like elastomers with molecularly encoded strain-adaptive stiffening and coloration, Science 359 (2018) 1509-1513.

[30] A.V. Dobrynin, J.M.Y. Carrillo, Universality in nonlinear elasticity of biological and polymeric networks and gels, Macromolecules 44 (2011) 140-146.

[31] J.M.Y. Carrillo, F.C. MacKintosh, A.V. Dobrynin, Nonlinear elasticity: from single chain to networks and gels, Macromolecules 46 (2013) 3679-3692.

[32] S.E. Webber, Polymer micelles: an example of self-assembling polymers, J. Phys. Chem. B 102 (1998) 2618-2626.

[33] A.M. Mayes, M.O. de la Cruz, Microphase separation in multiblock copolymer melts, J. Chem. Phys. 91 (1989) 7228-7235.

[34] E.B. Zhulina, M. Adam, I. LaRue, S.S. Sheiko, M. Rubinstein, Diblock copolymer micelles in a dilute solution, Macromolecules 38 (2005) 5330-5351.

[35] I. LaRue, M. Adam, E.B. Zhulina, M. Rubinstein, M. Pitsikalis, N. Hadjichristidis, D.A. Ivanov, R.I. Gearba, D.V. Anokhin, S.S. Sheiko, Effect of the soluble block size on spherical diblock copolymer micelles, Macromolecules 41 (2008) 6555-6563.

[36] F. D'Agosto, J. Rieger, M. Lansalot, RAFT-mediated polymerization-induced self-assembly, Angew. Chem. Int. Ed. 59 (2020) 8368-8392.

[37] J. Zheng, S. Jung, P.W. Schmidt, T.P. Lodge, T.M. Reineke, 2-Hydroxyethylcellulose and amphiphilic block polymer conjugates form mechanically tunable and nonswellable hydrogels, ACS Macro Lett. 6 (2017) 145-149.

[38] H. Kamata, Y. Akagi, Y. Kayasuga-Kariya, U. Chung, T. Sakai, “Nonswellable” hydrogel without mechanical hysteresis, Science 343 (2014) 873-875.

[39] S. Nakagawa, X. Li, H. Kamata, T. Sakai, E.P. Gilbert, M. Shibayama, Microscopic structure of the “nonswellable” thermoresponsive amphiphilic conetwork, Macromolecules 50 (2017) 3388-3395.

[40] H. Guo, N. Sanson, D. Hourdet, A. Marcellan, Thermoresponsive toughening with crack bifurcation in phase-separated hydrogels under isochoric conditions, Adv. Mater. 28 (2016) 58-64.

[41] Z. Guo, G. Zhang, F. Qiu, H. Zhang, Y. Yang, A.-C. Shi, Discovering ordered phases of block copolymers: new results from a generic fourier-space approach, Phys. Rev. Lett. 101 (2008) 028301.

[42] M.W. Matsen, M. Schick, Stable and unstable phases of a diblock copolymer melt, Phys. Rev. Lett. 72 (1994) 2660-2663.

[43] E. Helfand, Y. Tagami, Theory of the interface between immiscible polymers, Polymer Letters 9 (1971) 741-746.

[44] S. Yu, X. Piao, N. Park, Topological hyperbolic lattices, Phys. Rev. Lett. 125 (2020) 053901.

[45] P.J. Flory, Principles of Polymer Chemistry, Cornell University Press, New York, 1953.

[46] J.R. Fried, Polymer Science and Technology, Pearson Education Press, United States of America, 2014.

[47] L.R.G. Treloar, The Physics of Rubber Elasticity, Oxford University, New York, 1975.

[48] V. Karimkhani, M. Vatankhah-Varnosfaderani, A.N. Keith, E. Dashtimoghadam, B.J. Morgan, M. Jacobs, A.V. Dobrynin, S.S. Sheiko, Tissue-mimetic dielectric actuators: free-standing, stable, and solvent-Free, ACS Appl. Polym. Mater. 2 (2020) 1741-1745.

[49] S.S Sheiko, A.V. Dobrynin, Architectural code for rubber elasticity: from supersoft to superfirm Materials, Macromolecules 52 (2019) 7531-7546.